Chapter

Energy Storage in PCM Wall Used in Buildings' Application: Opportunity and Perspective

Majdi Hazami, Farah Mehdaoui, Hichem Taghouti, Marco Noro, Renato Lazzarin and AmenAllah Guizani

Abstract

This chapter deals with the investigation of the effect of a PCM wall on building indoor thermal comfort. To achieve this objective, an experimental framework was installed in the laboratory of thermal processes in Borj Cedria, Tunisia, which is essentially composed of a test cell having the dimension (0.5, 0.5, 0.5 m^3) conceived with a new structure of wallboards. One of the sides of the test cell is a cavity filled with PCM-27, which represents the PCM wall. A numerical investigation by using specific FORTRAN program was also achieved to solve the energy and the exergy mathematic relations to evaluate the PCM wall performances. TRNSYS simulation program was also achieved to simulate the behavior of the integration of the PCM wall in a typical modern house according to Tunisian scenario. It is found that during the hottest period of the day, the temperature of the tested room with PCM wall achieves 25°C, while that without PCM wall exceeds 27°C. During the night, the temperature of the tested room, with PCM wall, decreases in the value of 20°C. It was also found that during the night, the kid's room with PCM wall is reduced by 8°C.

Keywords: PCM wall, building, thermal storage, FORTRAN, TRNSYS

1. Overview

Nowadays, the building sector has become the main consumer of energy in the developed countries. Taking the EU as an example, the building sector accounts for around 40% of the total CO_2 emissions. In Tunisia, the building sector consumes about 30% of the total final energy and is consumed by domestic water heating systems and air conditioning equipments (**Figure 1**) [1]. In order to reduce the energy consumption in buildings and to improve the thermal comfort of occupants, many researchers are focusing on storing of the thermal energy excess as latent heat by using specific phase change material (PCM). PCM may be integrated into the construction material in three ways: by direct incorporation, impregnation or encapsulation. It has been shown that the incorporation of the microencapsulated PCM into the building material is a particularly attractive technology. Recently, many experimental investigations have been conducted about the incorporation of the microencapsulated PCMs into different building elements, such as into plaster, cement, concrete walls or concrete floors. These investigations were aimed to assess

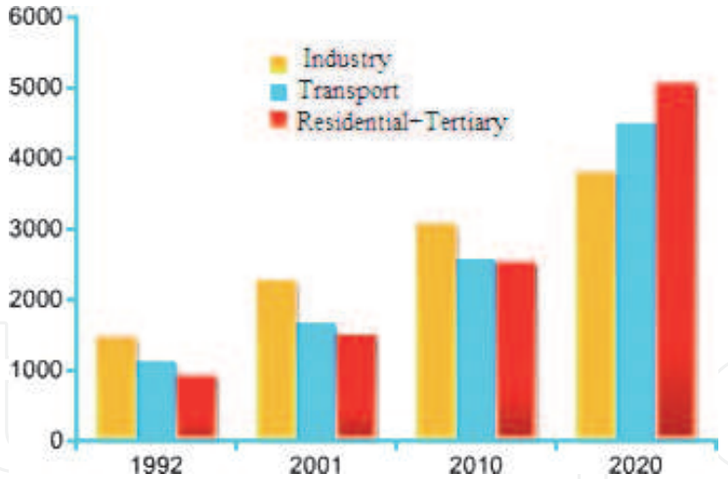

Figure 1.
The rates of energy expenditure in Tunisia (Mehdaoui et al. [1]).

the potential of PCM integration in walls and/or building envelopes to increase their thermal inertia to improve their energy performance [2–7]. In this context, Soares et al. [8] proposed the study of the incorporation of PCM drywalls in lightweight steel-framed building envelop. The authors evaluated the impact of PCM drywalls in the annual and monthly heating and cooling thermal performances and energy savings. It was seen that the energy savings due to PCM drywall incorporation range from 46 to 62%. Navarro et al. [9] studied the incorporation of the PCM inside the concrete core slab for cooling purposes. In this context, a prefabricated concrete slab incorporating PCM was used as internal separation inside the building. The results show that the energy savings in building were registered between 30 and 55%. Solgi et al. [2] presented that PCMs have a great influence on enhancing the performance of night purge ventilation and cooling load reduction of buildings in hot-arid climate. It was found that paraffin with 27°C melting point permits the reduction of about 47% in cooling energy. A performance of a collector storage wall system using PCMs was investigated by Zhou et al. [10]. PCM slabs were integrated in the gap-side wall surface to enhance the heat storage. The test was carried out for a whole day with charging period of 6.5 h and discharging period of 17.5 h. They investigated the variations of surface temperature as well as the indoor temperatures. It was found that the indoor temperature was about 22°C during the whole discharging period under given conditions. Barzin et al. [11] presented an experimental study dealing with the building's space cooling by using PCM energy storage in combination with night ventilation. Hence, two experimental tests were achieved: one with PCM-impregnated gypsum boards and the other with normal gypsum board. The result of the experimental investigation shows that substantial electricity saving is about to 73%. Sajjadian et al. [12] presented the study of the potential of using PCMs to reduce domestic cooling energy loads for current and future UK climates. The study used simulations of a high performance detached house model with a near Passivhaus Standard in London, where the impact of climate change effect is predicted to be significant. It was shown that appropriate levels of PCM, with a suitable incorporation mechanism into the building construction, have significant advantages for residential buildings in terms of reducing total discomfort hours. In this context, Royon et al. [13] studied the optimization of PCM implanted in a floor panel envelope of buildings. The study is mainly based on numerical investigation. The numerical results were confronted to experimental ones with the same boundary conditions in order to validate the model. Łukasz et al. [14] presented a parametric study of the thermal performance characteristics of thermal energy storage unit based on PCM integrated in building structure. In order

to perform the analysis of the storage unit, a simulation program was developed. Using the program, many computer simulations were performed. In their work, Łukasz et al. presented important conclusions regarding the selection of PCM, and mainly its melting temperature range was formulated. Xiaoming et al. [15] studied the potential of exploiting ventilation systems with thermal energy storage (TES) and by using phase change materials (PCMs) for space cooling in air conditioned buildings during the summer. A dynamic computational model was achieved in order to simulate the indoor thermal environment and energy consumption of the room. The results showed that the electricity energy saving ratio (ESR) by using the TES system over the base case ranges between 16.9 and 50.8%, while considering the conventional NV system, the ESR ranges between 9.2 and 33.6%. Stropnik et al. [16] presented a study a system assuring self-sufficient heating and cooling of building from solar energy and interconnection between PV, electrical storage, heat pump, thermal energy storage and building energy management system. They showed that with such a smart energy system the almost zero-energy buildings can be reached in residential sector. The results show that thermal energy storage unit with integrated PCM modules supplies desired quantity of water temperature for longer period of time. Pushpendra et al. [17] presented a detailed review of various approaches to integrate the PCM in the building envelope. They showed that this method not only improves the indoor thermal behavior of the buildings but also reduces the cooling load without or little compromise with the mechanical strength of the building structure. They studied also the effect of the PCM integration on indoor thermal behavior and reduction in cooling load. They presented also an investigation of various materials used for making containers for encapsulation and it was also investigated. From the studied technologies, a great attention was given to investigate the effects of design parameters on thermal performances of PCM radiant floor heating system integrated in buildings. In this context, Li [18] proposed a numerical investigation aiming at the evaluation of the thermal performance of different kinds of roofs with and without PCM installed in Northeast China. They showed that the effect of transition temperature and latent heat of PCM on the thermal performance of roofs is relatively weak, compared with the roof slope, PCM layer thickness and absorption coefficients of external roof surface. In 2015, Joulin et al. [19] proposed an experimental and a numerical investigation of a PCM-27 conditioned in a rectangular container located between two heat exchangers. It was found that the PCM needs about 1.48 h to melt during the charging process. The evaluation of the effect of the integration of PCM inside a building was also studied with experimental and simulation methods by Huang et al. [20]. They showed that the PCM floor is able to supply about 37.7 MJ heat for 16 h in a building. In the same context, Prieto et al. [21] concluded that the integration of solar collectors holding PCM as storage material provided about 18–23% of total daily thermal energy needs of the building. Krese et al. [22] present also an experimental study of a small-scale wall composite containing PCM-27. The result of the investigation indicates that the heat recovery throughout the night is about 25 W/m^2.

2. Experimental methodology and framework

The aim of the research presented in this chapter is to evaluate the effectiveness of a PCM wall used as a storage medium in reducing the building's air temperature and in improving the occupant's thermal comfort in a Tunisian real house. A specific experimental framework was presented to characterize the PCM wall behavior during the storage and the discharging process (**Figure 2**). In this experimental

Figure 2.
PCM wall filled with Paraffin-27.

investigation, a PCM wall was installed in a test cell (**Figure 3**). A framework was installed to follow the indoor air temperatures of the various rooms of the house (with and without PCM). Thirteen T-type copper-constantan thermocouples firstly calibrated with a measurement inaccuracy of ±0.2°C were incorporated to PCM wall at the front surface, inside PCM, the back surface and inside the test cell as shown in **Figure 4**. Between the exchanging plates, T-type thermocouples are inserted in both sides of the Plexiglas container to measure the temperature fields on each side of the PCM wall. T-type thermocouples were previously calibrated by using the comparative method. **Figure 4** shows the positions of all thermocouples inside the test cell.

The measurement test was continued for 14 consecutive days during February and March 2016 (from 25/02/2016 to 13/03/2016) to evaluate PCM wall performance. The temperature was measured at front surfaces of PCM wall, at back surfaces of PCM wall, inside the PCM and inside the test cell. The method adopted in the investigation consisted of imposing heating flux (lamp of 120 W) on the exposed PCM wall of the test cell. The simultaneous measurements of the temperature evolution and the heat flux exchanged during charging and the discharging process were accomplished to evaluate the PCM wall thermal performances. A primary experimental test was conducted in the laboratory to determine the characteristics of the phase change material (PCM) during the melting phase. PCM is initially in the solid state at the ambient temperature of the room, 22°C. Then, the right side of the PCM wall was heated by using a special lamp of 120 W held at a distance of 10 cm to ensure the uniformity of heat over the PCM wall surface. By

Figure 3.
The test cell.

Figure 4.
The position of the 13 thermocouples inside the test cell.

using the data acquisition system, the temperature change at the interior of PCM wall during the charging process is followed. In the second test, the lamp was extinguished and then the PCM temperature fields were followed to evaluate the heat exchanged through the PCM wall during the discharge process.

3. PCM wall numerical characterization

A numerical investigation by using specific FORTRAN program was achieved to solve the energy and the exergy mathematic relations to evaluate the PCM wall performances by determining the melting phase proprieties (velocity, isotherm, melting front evolution, etc.).

The proposed numeric investigations describe the heat transfer phenomena inside the PCM wall and evaluate its thermal behavior and effects on test cell ambiance. It allows also the appraisal of the energy and exergy stored during the charging process and to evaluate the thermal characteristics. The considered assumptions are the flow is two-dimensional and laminar, the expansion of the PCM is negligible and the phase change is isothermal. The PCM wall is subjected to an imposed temperature superior to the melting temperature of PCM-27 (**Figure 5**).

The other walls are maintained adiabatic (**Figure 5**). Considering the mentioned assumptions:

- The continuity equation is given by [1, 23]:

$$\frac{\partial u}{\partial x} + \frac{\partial v}{\partial y} = 0 \tag{1}$$

- The quantity of movement relations are given by [1, 23]:

$$\rho_l \frac{\partial u}{\partial t} + \rho_l \left(\frac{\partial u u}{\partial x} + \frac{\partial u v}{\partial y} \right) = -\frac{\partial p}{\partial x} + \mu_l \left(\frac{\partial^2 u}{\partial x^2} + \frac{\partial^2 u}{\partial y^2} \right) + Bu \tag{2}$$

$$\rho_l \frac{\partial v}{\partial t} + \rho_l \left(\frac{\partial u v}{\partial x} + \frac{\partial v v}{\partial y} \right) = -\frac{\partial p}{\partial y} + \rho_l g + \mu_l \left(\frac{\partial^2 v}{\partial x^2} + \frac{\partial^2 v}{\partial y^2} \right) + Bv \tag{3}$$

In the Boussinesq approximation, the source terms B_u and B_v that appear in the momentum Eqs. (2) and (3) are used to account for this buoyancy force when the PCM is solid. The technique used to cancel the velocity introduces a Darcy term [1].

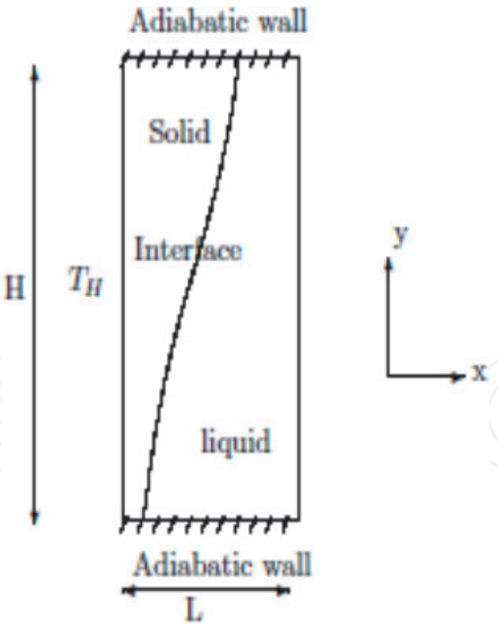

Figure 5.
Boundary conditions through the PCM wall.

$$B = -C\frac{(1-H^2)}{(H^3+b)} \tag{4}$$

The constant C is chosen so that it is high enough to cancel the velocities in the solid region and a low number b is introduced to avoid a division by zero in the case of a zero liquid fraction: where b = 0.001 is a small computational constant used to avoid division by zero, and C is a constant reflecting the morphology of the melting front. A value of C = 10^5 has been used in the literature [1]. The liquid fraction (H) is given by [1, 24].

$$H = \begin{cases} 0 & if \quad T < T_{melting} \\ ]0,1[& if \quad T = T_{melting} \\ 1 & if \quad T > T_{melting} \end{cases} \tag{5}$$

The energy equation is written as [25, 26].

$$Cp_{eq}\frac{\partial T}{\partial t} = \lambda_{eq}\left(\frac{\partial^2 T}{\partial x^2}+\frac{\partial^2 T}{\partial y^2}\right) + Cp_{eq}\left(u\frac{\partial T}{\partial x}+v\frac{\partial T}{\partial y}\right) \tag{6}$$

Cp_{eq} and λ_{eq} that appear in Eq. (8), respectively, represent the equivalent volume capacity (J/K) and the equivalent thermal conductivity ($W/m\ K$) of the two solid and liquid phases of PCM, such as:

$$Cp_{eq} = \sum \theta_i \rho_i (Cp)_i \tag{7}$$

$$\lambda_{eq} = \sum \theta_i \lambda_i \tag{8}$$

The term θ_i that appears in Eqs. (9) and (10) is a quantity related to the H value, which provides information on the state-owned PCM whether liquid or solid. The thermal and dynamic initial conditions are, *respectively, u = v = 0 (once t = 0) and* $T = T_0 = 288.15\ K$.

- In order to account for the phase change process happening when the PCM is melting, the energy balance was applied at the interface as follows [27, 28]:

$$k_s \vec{\nabla} T_s - k_l \vec{\nabla} T_l = \rho L \frac{dX}{dt} \tag{9}$$

- Since the phase change of pure substances occur at a single temperature, the temperatures of liquid and solid at the interface is given by [1]:

$$T_l = T_s = T_i \tag{10}$$

where the subscripts s and l stand for the solid and liquid phase, L is the latent heat (enthalpy) of fusion, and X is the position of the melting interface.

- The Plexiglas cavity was partially filled with PCM-27 heated by a lamp placed at 0.1 m. The lamp imposes the uniformity of heat and temperature, T_H, on the directly exposed PCM wall surface. The condition of adhesion was used to express the velocity fields. The thermal and the dynamic bounder conditions in the PCM vertical enclosure are given by the following expressions:

- The left vertical side of area ($x = L$, y, t) is maintained to a temperature T_H upper to the PCM melting temperature:

$$u(x = L, y, t) = v(x = L, y, t) = 0 \tag{11}$$

$$T(x = L, y, t) = T_H \tag{12}$$

- The right vertical side of the PCM wall ($x = 0$, y, t) of the area is maintained adiabatic:

$$u(x = 0, y, t) = v = (x = 0, y, t) = 0 \text{ and } \partial t/\partial x = 0 \tag{13}$$

- The horizontal walls of the domain are maintained adiabatic (x, $y = 0$, t) and (x, $y = H$, t):

$$u(x, y = 0, t) = v(x, y = 0, t) = 0, \frac{\partial T(x, y = 0, t)}{\partial y} = 0 \tag{14}$$

$$u(x, y = H, t) = v(x, y = H, t) = 0, \frac{\partial T(x, y = H, t)}{\partial y} = 0 \tag{15}$$

3.1 Energy and exergy analysis

- The energy stored, E_S, in the PCM wall is given by [25]:

$$E_S = M_{PCM-27}.C_{PCM-27}.(T_{PCM,F} - T_{PCM,1}) + M_{PCM-27}.L \tag{16}$$

where $M_{PCM\text{-}27}$ (kg) represents the PCM-27 mass, $C_{PCM\text{-}27}$ (kJ/kg°C) represents the specific heat of PCM-27, $T_{PCM,\ I}$ (°C) is the initial temperature of PCM, $T_{PCM\text{-}27,\ F}$ (°C) is the final temperature of PCM, L (kJ/kg) is the latent heat of fusion, $A_{PCM\ wall}$ (m^2) is the aperture area of the PCM wall, T_{cell} (°C) is the test

cell temperature, and $h_{PCM\text{-}27}$ (W/m^2°C) is the heat transfer coefficient of PCM-27.

Energy input during charging is given by:

$$E_{ic} = I.A_{PCM\,wall} \tag{17}$$

where I (W/m^2) is the irradiance intensity of the lamp and $A_{PCM\ wall}$ (m^2) is the PCM wall area.

- The energy efficiency of the PCM wall during the charging and the discharging processes are given by:

$$\eta_c = \frac{E_0}{E_{ic}} \text{ and } \eta_d = \frac{E_S}{E_0} \tag{18}$$

where E_0 is the energy transferred to the PCM wall.

- The overall exergy transferred to the PCM wall is given by [29, 30]:

$$EX_0 = M_{PCM-27}.C_{PCM-27}.\left(T_f - T_i\right) + M_{PCM-27}.L.\left(1 - \frac{T_a}{T_s}\right) - M_{PCM-27}.T_a.C_p.\ln\left(\frac{T_f}{T_i}\right) \tag{19}$$

where $T_a(K)$ is the ambient temperature and $T_s(K)$ is the temperature of sun.

- Exergy input during the thermal storage is given by [30]:

$$EX_{ic} = I.A_{PCM\,wall}.\left(1 - \frac{T_a}{T_s}\right) \tag{20}$$

- Exergy efficiency of the PCM wall during the thermal storage and the thermal discharging are respectively given by:

$$\Psi c = \frac{EX_0}{EX_{ic}} \text{ and } \Psi_d = \frac{E_S X}{EX_0} \tag{21}$$

4. Numerical results

4.1 Validation of the numerical model

This section is devoted to the obtained experimental results and their comparison with experimental data. The validation of the numerical model used in this study was performed by following the temperature changes inside the PCM wall and the melting front states during the charging process. The numerical results were compared with the experimental temperature data recorded in the laboratory during the same period between February 25 and March 13, 2016. **Figure 6** shows the temperature evolution in the vertical plane x = L/2 vs. local time for the low position (a) (y = 1 cm) and the high position (b) (y = 7.5 cm) of the PCM wall. **Figure 6a** shows that the numerical results are quite similar to the experimental measurement. Indeed, the difference between the simulated and the measured values of the temperature at the bottom of PCM is about 0–4°C. It is also seen that in a higher position of PCM wall (**Figure 6b**) the experimental and numerical results of

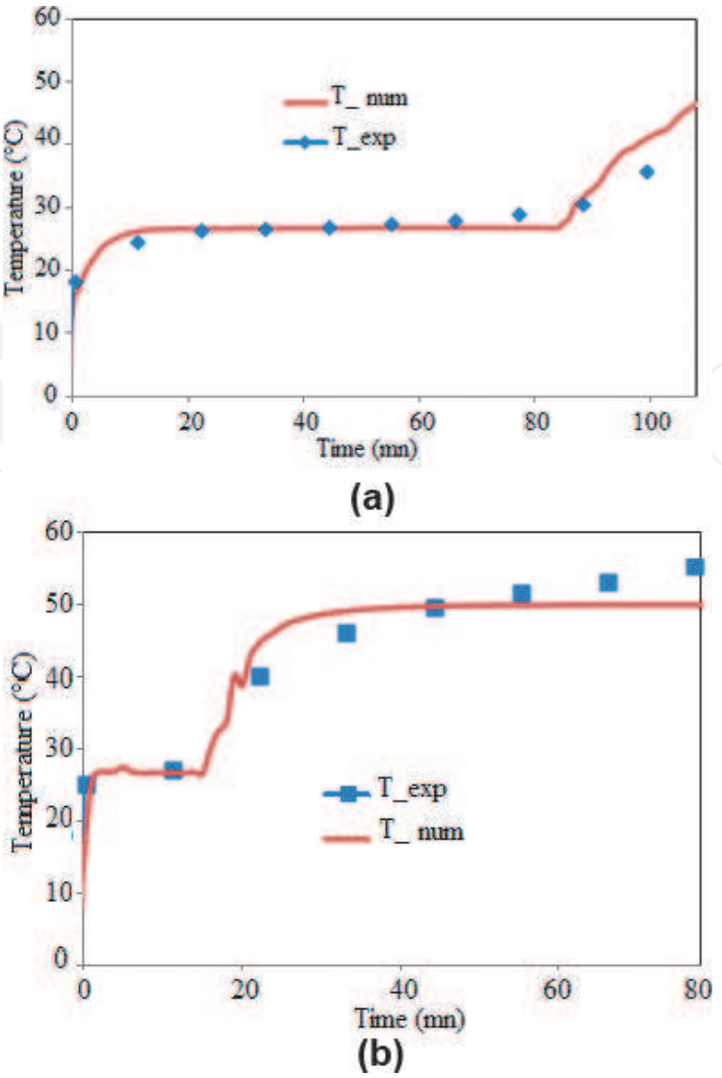

Figure 6.
The simulated and the experimental temperature profile inside the PCM wall for two different times: (a) 4000 and (b) 6000 s.

temperature obtained show an acceptable agreement, of about 0–5°C. It is concluded that the numerical model permits the simulation of the PCM wall thermal behavior with an acceptable accuracy.

4.2 Exploitation of the numerical model

Figure 7 shows the variation of the energy and the exergy stored in the PCM wall during storage process. It is found that the recovered energy incessantly increases vs. charging time. It ranges between 95 and 780 W. This variation takes roughly 130 min and then the energy stored reaches a maximum, which value is due to the fact that the test cell temperature also fluctuates that is in the range of 22–24°C (**Figure 7**). On the other hand, it is found that the exergy stored grows with the charging time. However, it is seen that the exergy is lesser than the stored energy. It varies between 50 and 460 W.

Figure 8 shows the variation of the energy and exergy efficiencies of PCM wall during the charging process. It is seen that the PCM wall performance increases gradually from 10 to 95%. **Figure 9** shows the variation of the energy and exergy efficiencies of PCM wall during the discharging process. It is seen that the PCM wall performance decreases regularly from 100 to 10%. It is found that the energy and exergy efficiencies are more important than the charging process. It is also seen that

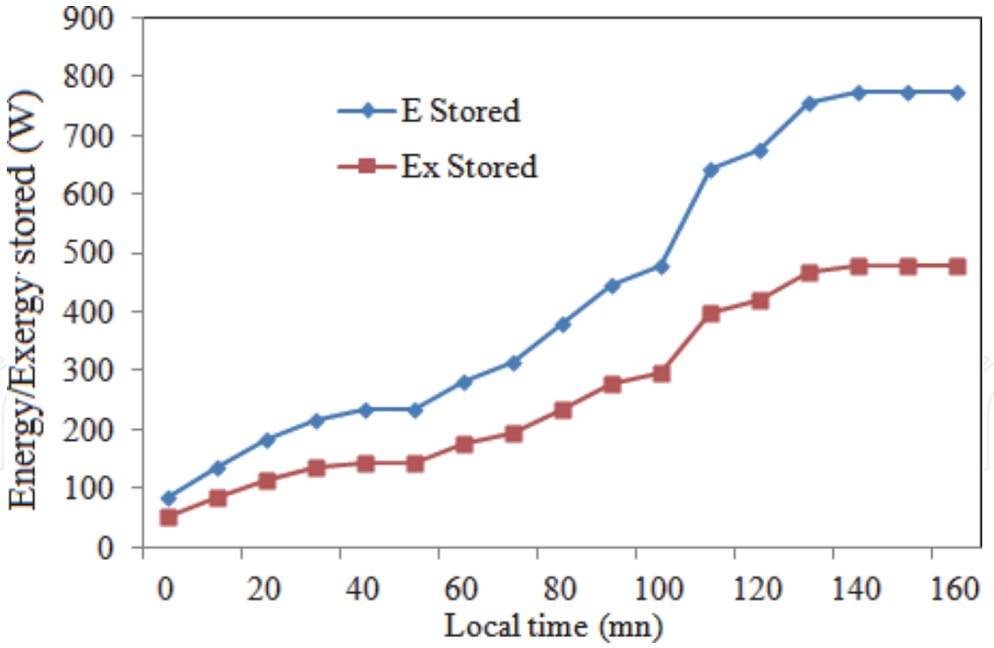

Figure 7.
Thermal energy and exergy changes during the charging process.

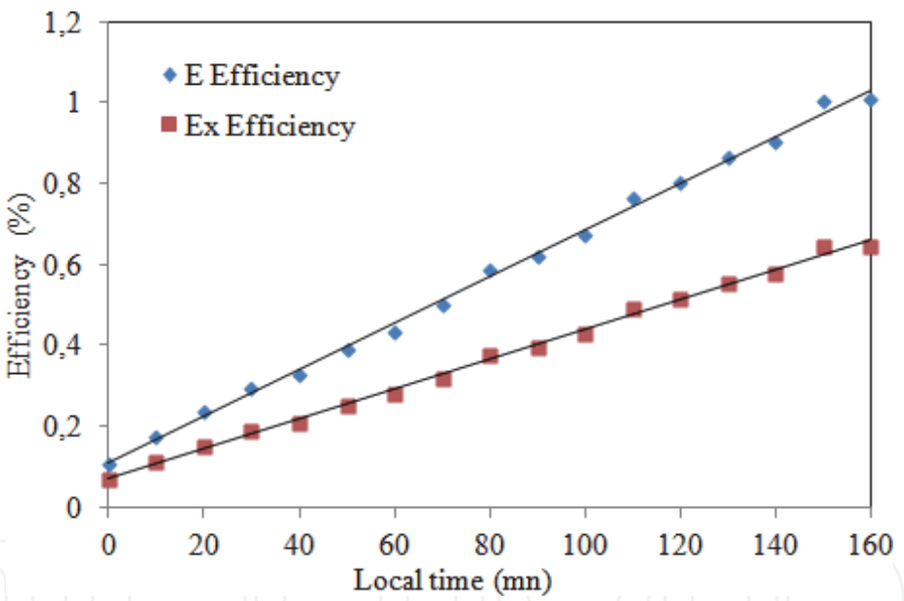

Figure 8.
Thermal energy and exergy efficiency changes during the storage stage.

the exergy efficiency is always found to be lower than the energy efficiency, which is due to the consideration of the losses/irreversibility during exergy analysis, which ultimately gives the information about the quality of energy or available energy. On the other hand, the energy efficiency is all about the quantity of energy rather than quality as it does not consider the losses/irreversibility in the analysis. Both the efficiencies are found to be decreasing with increasing loads. This is due to the fact that backup time is inversely proportional to the increase of the heating load.

In **Figure 10**, the evolution of the melting front inside the vertical enclosure for two different instances (4000 and 6000 s) is represented. At the beginning of the heating process, the PCM-27 inside the vertical enclosure was in solid phase. Then, we detected the presence of two distinct phases: a liquid phase and a solid phase separated by melting front. It was seen that the ending of the melting process was observed after 6000 s. It is also seen that the liquid in the vicinity of the directly

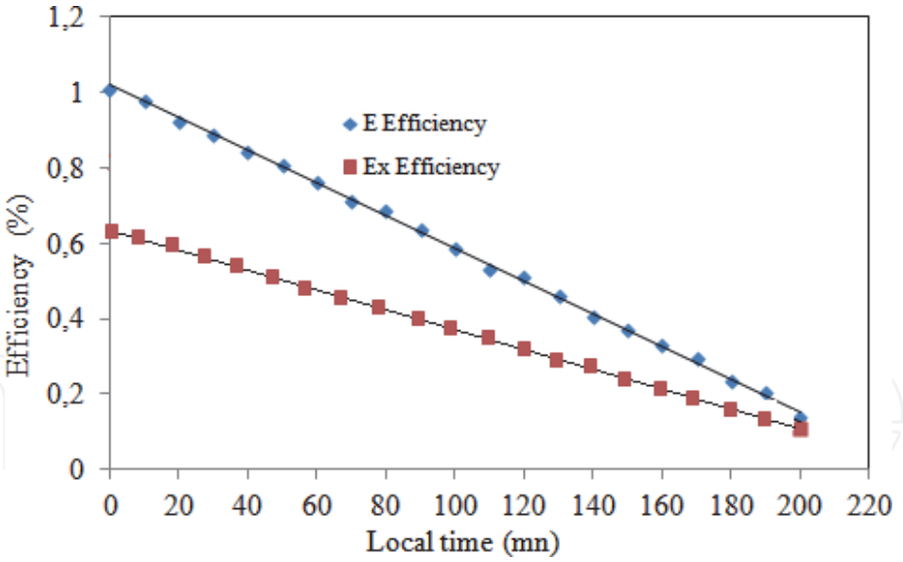

Figure 9.
Thermal energy and exergy efficiency changes during the discharging phase.

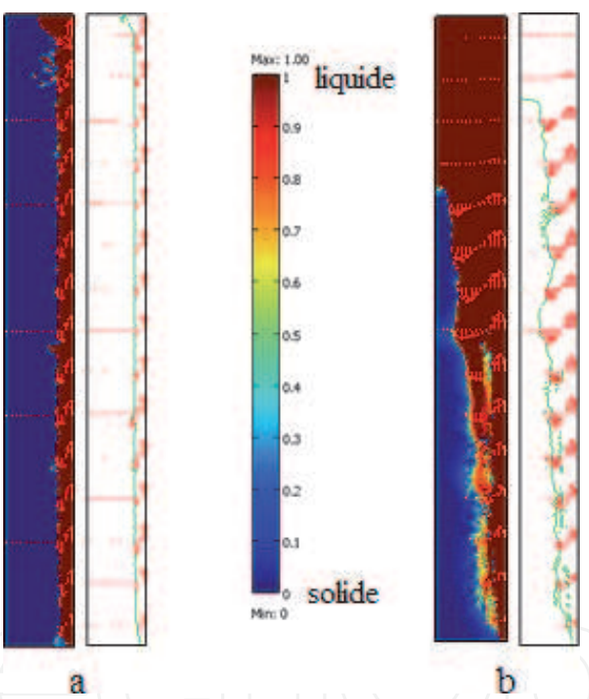

Figure 10.
Evolution of the melting front and the velocity fields inside the PCM wall for two different instances ((a) 4000 and (b) 6000 s).

heated side of the PCM wall acquires heat, causing the temperature increases of the PCM-27. Consequently, a decrease of PCM-27 density was noted, which ascends along the heated PCM wall. At the top of the test cell, the velocity of the fluid is very important, so the liquid descends along the solid-liquid interface. During its descent, it loses its heat to the cold interface. At the bottom of the interface, the fluid is cold, and the temperature of the melting rate gradients is low. A blocking of the thermal transfers leading to the slowdown of the interface movement occurs in the latter region. In the liquid phase, PCM-27, which is at the top of the field, has a slightly higher temperature than the bottom of the cavity temperature. It is noted that the interface movement forms a contour from the bottom of the cavity, along the heated side to descend on the other side of the PCM wall. It is seen that as convection increases, the melting rate increases in the upper part of the PCM wall.

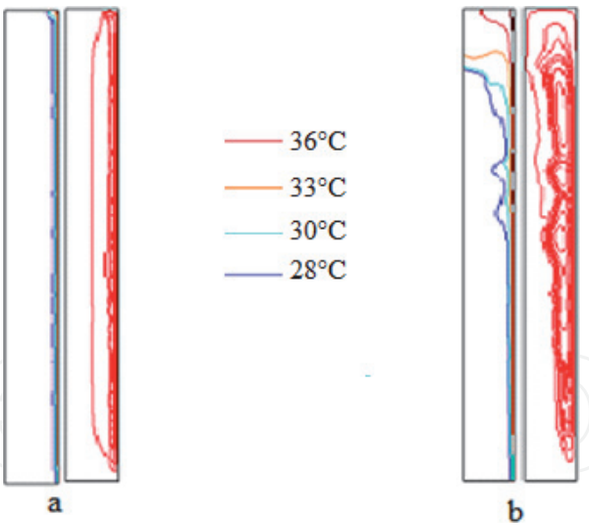

Figure 11.
Isothermal and current lines inside the PCM wall for two different instances ((a) 4000 and (b) 6000 s).

This is explained by the fact that the paraffin in the vicinity of the PCM wall heated side acquires heat, which causes the climb of the upper part with a high speed and then the liquid paraffin descends along the solid-liquid interface.

Figure 11 shows the thermal and the dynamic behavior of the PCM-27 for two different instances (4000 and 6000 s). It was seen that at the beginning of the melting process, the interface is almost vertical, indicating the predominance of heat transfer by conduction mode. Isotherms remain vertical and parallel. Gradually as the convection increases, the melting rate increases in the upper portion of the interface. Therefore, the PCM-27 in the upper area has a higher temperature than the bottom of the cavity and the isotherms do not remain parallel. It is noted also that these movements are not made of the plate toward the solid–liquid interface. They form an outline by gravity from the bottom of the cavity, along the plate to descend on the other side on the solid-liquid interface.

5. Experimental investigation according to Tunisian scenario

An experimental framework and procedure were accomplished in the laboratory in order to evaluate the PCM wall thermal performances, in particular its capacity to store the heat and to moderate internal test cell temperature. The experimental framework considered for the investigation of the thermal performances of the PCM wall comprises essentially a test cell with the dimensions $0.5 \times 0.5 \times 0.5\ m^3$ and managed to imitate a test room. Each sides of the test cell have the dimensions: 0.22 m length, 0.22 m width and 0.026 m thickness. One side of the conceived test cell is fixed with a Plexiglas parallelepiped-shaped container with a size of $22 \times 22 \times 2.6\ mm^3$. The sides of the PCM wall are fixed with the epoxy resin to form a strong bond. Then, the Plexiglas container was field with paraffin-27, which melts at 27°C with a high latent heat storage capacity (about 110 J/g). Upon PCM solidification, a $7\ 10^{-2}$ m free space was left from the top of Plexiglas container to accommodate volume changes and release trapped air during successive melting and solidification phases. A 120-W incandescent lamp is used for heating the exposed side of the PCM wall. The thermophysical properties of the PCM-27 are given in **Table 1**.

Data acquisition is achieved by an autonomous acquisition device controlled by a Lab VIEW program adapted to measure temperature fluctuations during melting

Thermal conductivity (W/m·K)		Heat capacity (kJ/kg·K)		Density (kg/m^3)		Enthalpy of fusion (kJ/kg)	Melting temperature (K)
Solid	Liquid	Solid	Liquid	Solid	Liquid		
1.05	0.58	1.42	2.22	1530	1710	172.42	300.15

Table 1.
Thermophysical properties PCM-27 [30].

processes. It acquires the output signals from the thermocouples, digitizes, treats them and then saves the results. Data are directly collected with the help of an interface network between the measurement station and a computer equipped with application software. Storing data is performed with a regular pitch, equal to 60 s, in the form of text file. **Figure 12** shows the entire device and framework. Thirteen T-type copper-constantan thermocouples firstly calibrated with a measurement inaccuracy of ±0.2°C were incorporated to PCM wall at the front surface, inside PCM, the back surface and inside the test chamber as shown in **Figure 10**. Between the exchanging plates, thermocouples (T-type) are inserted on both sides of the sample to measure the temperature fields on each side of the PCM wall. The thermocouples were fixed at the front and back surface with strong white tape and were shielded from direct irradiation.

The experimental investigation was conducted for 14 consecutive days in September 2015 (from 23/09/2015 to 07/10/2015) to evaluate PCM wall performance. The temperature was measured at front surfaces of PCM wall, at back surfaces of PCM wall, inside the PCM and inside the test cell. The method adopted in the investigation consisted of imposing heating flux (lamp of 120 W) on the exposed PCM wall of the test cell. Simultaneous measurements of the temperature variations and heat flux exchanged during charging and discharging processes were accomplished to evaluate the PCM wall thermophysical properties [29, 30]. The experimental test conducted in the laboratory aims to determine the PCM characteristics during the storage phase. The test starts at 9:00 am and continues until the total melting of PCM-27. PCM is initially in the solid state at the ambient temperature of the room, which is about 22°C. Then, the right side of the PCM wall was heated by using a special lamp with a thermal power of about 120 W. The lamp was held at a distance of 10 10^{-2} m to guarantee the uniformity of heat over the entire PCM wall area. By using the data acquisition system, the temperature variation at the interior of PCM wall during the storage stage was followed. To evaluate the heat

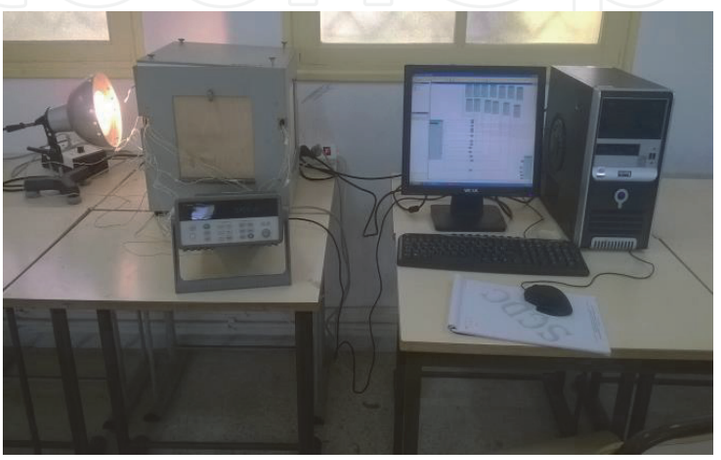

Figure 12.
Experimental device and framework.

exchanged through the PCM wall during the discharge process, the lamp was omitted and then the PCM temperature fields were tracked.

The result of the experimental tests permits the characterization of the PCM wall and the description of the test cell thermal behavior. **Figure 13** shows the temperature evolution of PCM-27 inside the wall during the charging and discharging processes along the vertical axis ($x = 10^{-2}$ m) (T1, T2, T3 and T4) and along the horizontal axis ($y = 7.5\ 10^{-2}$ m) (T5, T6, T7, T8 and T9). It is found that the PCM solidification process during the discharging phase takes more time than the storage stage. This is explained by the formation of a solid layer of paraffin in contact with the PCM wall sides, which make a thermal isolation and consequently slow down the crystallization in the other parts of the wall. It is seen that by the launch of the melting process all temperature profiles grow linearly up to 27°C. This phase corresponds to sensible heat storage in the solid PCM. Then, it is noted that during about 20 min of heating process with the lamp of 120 W all positions confess symmetrical temperature profiles, around 27°C. It is noted that PCM-27 temperature rises rapidly especially in the first 20 min of the melting process, which corresponds to the sensible storage process inside the PCM wall. Then, the PCM-27 temperature varies slowly between 27 and 29°C during the latent heat storage process. After about 40 min of heating by the lamp, the PCM-27 temperature increases to reach 50°C. **Figure 13** shows also that the temperature of thermocouples that are close to the heated side increases rapidly than those of the other sides. During this phase, the storage of heat is achieved by sensible process inside the melt PCM. After the melting process, it is noted that the different vertical positions inside the PCM wall ($y = 2, 8, 12$ and $18\ 10^{-3}$ m) presented a dissimilarity in the measured temperature. This delay is explained by the trajectory of the melting front of the solid–liquid interface, which merges firstly from the positions located above the PCM wall to the bottom. The duration of this phase varies between 110 and 40 minutes from one position to another according to the thermocouple on-axis position ($x = 10^{-2}$ m).

Figure 14 shows the variation of test cell air temperatures with and without PCM-27. The test was accomplished by exposing the PCM wall to the lamp of 120 W used as a heating load source. It is seen that during the charging phase the temperature profile inside the test cell with PCM wall is almost stable at 29°C. Indeed, the PCM wall permits the storage of the excess of heat supplied by the lamp. It is also

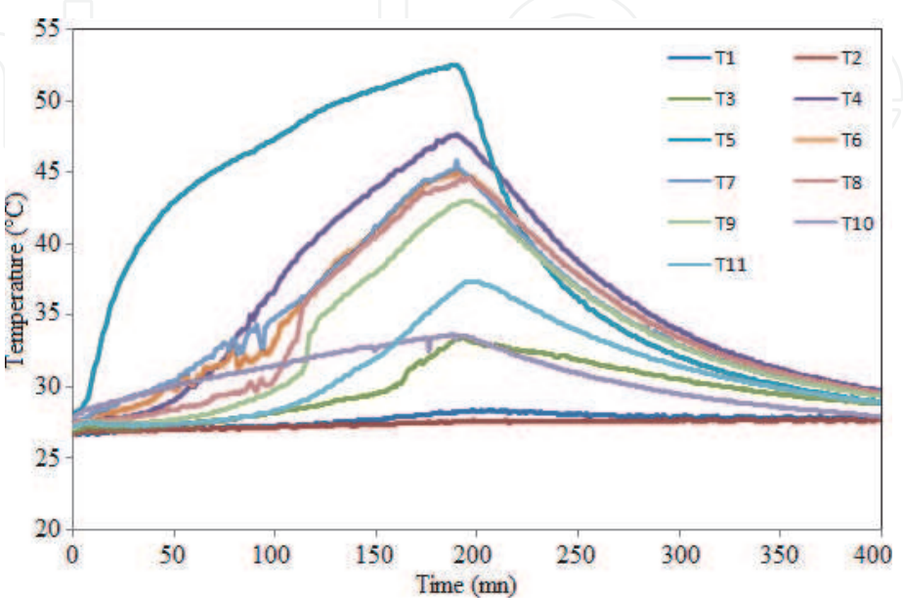

Figure 13.
Evolution of PCM temperature during charging and discharging phases.

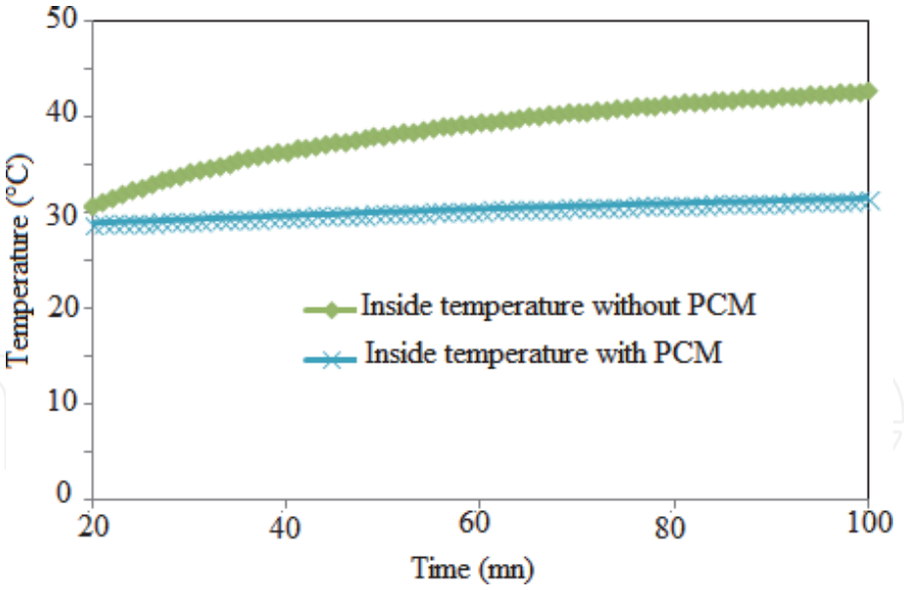

Figure 14.
Evolution of the temperature inside the test cell during the storage phase.

found that once the PCM wall is replaced by simple wooden wall the internal temperature of the test cell grows seriously from 29 to 40°C.

Figure 15 shows the temperature variation of the air inside the test cell with and without PCM wall during the discharging phase (cooling). As can be seen, the air temperature inside the test cell is stabilized around 21°C, which represents the ambient temperature, whereas with PCM wall, the air temperature inside the test cell decreases continuously with respect to time from 27 to 22°C. It is also noted that the temperature of the test cell with PCM is always higher than the temperature of the test cell without PCM. This shows the significance of using PCM inside the room and the temperature in the thermal comfort range can be maintained for a long time even with the heating load. Consequently, intruding of the PCM wall in the test cell presents a good potential to be applied for space conditioning.

To generalize the investigation, a simple room (kid's room) inside a typical modern house (**Figure 16**) in Tunis, Tunisia, is considered. The building is composed of five rooms with a floor area of 128 m^2. The technical specifications of the selected room are presented in **Table 2**. This scenario is archived by considering a

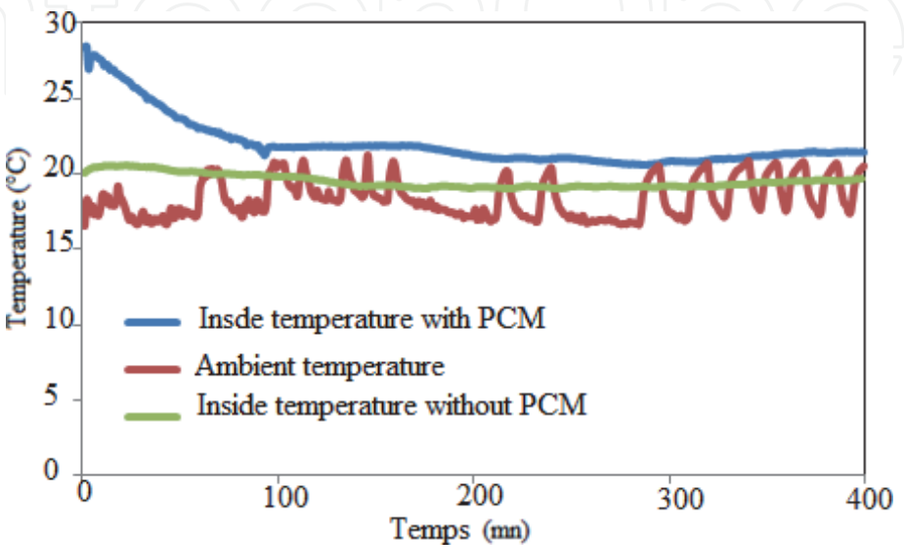

Figure 15.
Evolution of the temperature inside the test cell during the discharging phase.

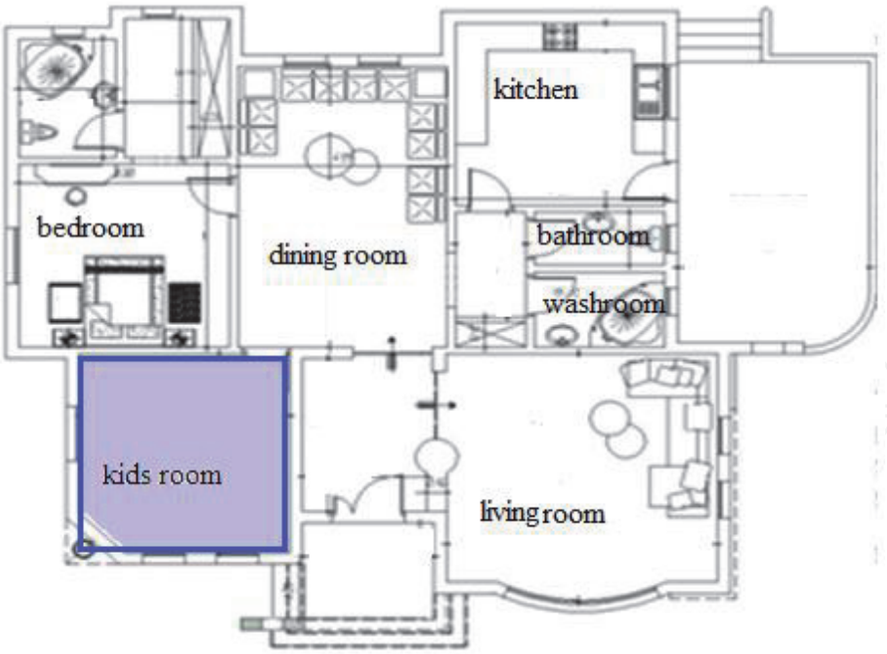

Figure 16.
The typical house plan used in this study.

Type	Layer	Thickness (m)	Conductivity (kJ/(h m K))	Density (kg/m^3)	Specific heat (kJ/kg K)
Wall	Brick	0.15	3.2	1800	1
	Concrete	0.15	7.56	2400	0.8
	Gypsum	0.05	0.75	1200	1
Ground	Concretes	0.06	4.06	1400	1
	Insulation	0.05	0.15	40	0.8
Roof	Concrete	0.24	7.56	2400	0.8

Table 2.
Structure and physical properties of the building structure.

TRNSYS program. The component of the TRNSYS model is the flat-plate solar collector (type73) used as a heat source, storage tank (type4c) and the building (type 56a). In this section, the integration of the PCM wall in the envelope of a typical Tunisian building is simulated by using TRNSYS. The main TRNSYS component used is Type 399, which models a PCM wall. Type 399 is designed to interact with Type 56a and can simulate a PCM wall located in any position within the tested room. It should be also noted that a new Type 399 models a pure PCM-27 that is assumed to go through its freeze/thaw process at constant temperature, to have a constant specific heat in the liquid phase and to have a constant specific heat in the solid phase. The basic architectural specification of the selected room used in Tunisian scenario is given in **Table 2**.

Figure 17 illustrates the evolution of the energy stored and destocked during four days, from January 1 to 4, 2015. During the day, the PCM wall stores a rate of heat brought by the solar collector, and this phase of storage is characterized by positive values of the energy. The latter forms a peak dependent on the period of sunshine and that can reach 1200 kJ m^{-2}. The heat accumulated during the day by the PCM wall will be restored to be used at the end of the day and during the night.

Figure 18 illustrates the variation of the temperature inside the selected room with and without integration of PCM wall during the period from January 1 to 4,

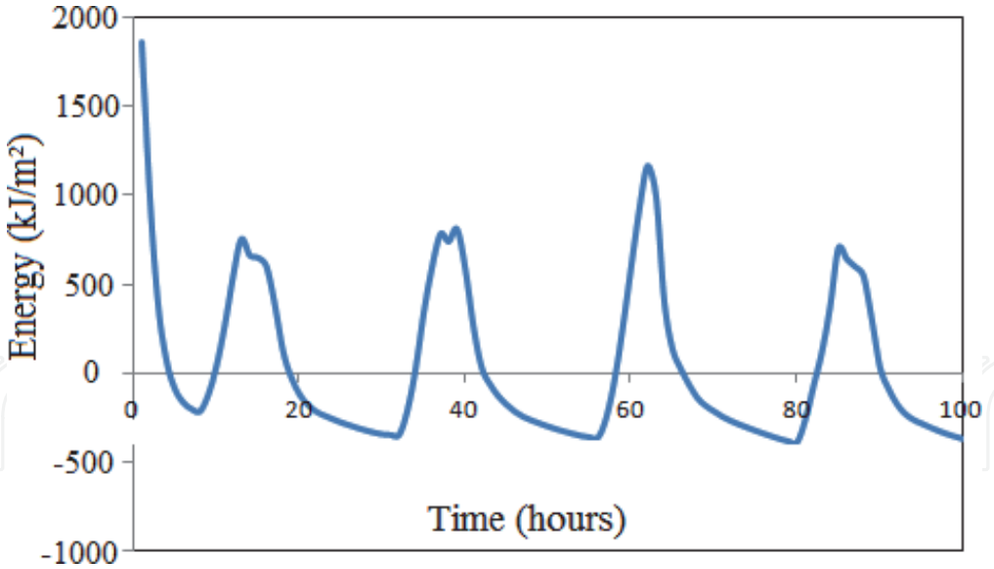

Figure 17.
Evolution of the energy stored in the PCM wall during the discharging phase.

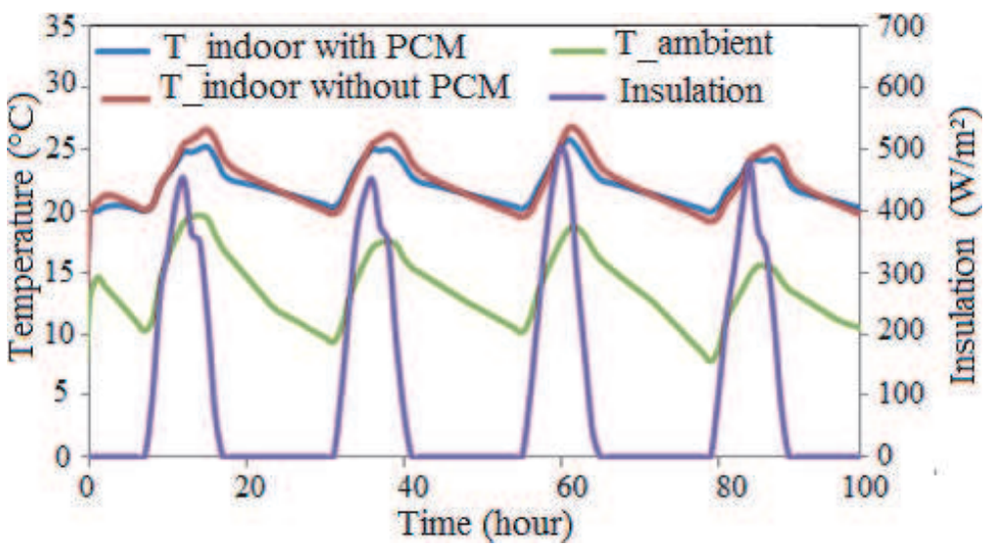

Figure 18.
Evolution of the ambient temperature inside the kid's room with and without PCM wall application.

2015. The outside temperature and the solar irradiation were also evaluated during the same period. During the hottest period of the day, the temperature of the tested room with PCM wall achieves 25°C, while that without PCM wall exceeds 27°C. During the night, the temperature of the tested room, with PCM wall, decreases in the value of 20°C. During the night, the temperatures for the system using the PCM wall become more marked, more of 1°C compared with that of the system without PCM wall. It is seen that the PCM wall performs its function of thermal shock absorber.

6. Conclusion

The objective of this chapter is to show the importance of using PCM as storage material in buildings and to study the thermal potential offered by the integration of a PCM wall to enhance the thermal comfort of the occupant by reducing the thermal fluctuation and by improving the thermal inertia of the buildings' envelop. Accordingly, an experimental prototype represented by a small-scale home

(0.5 × 0.5 × 0.5 m3) was conceived in our laboratory. The test cell was equipped with a PCM-27 vertical enclosure placed at one side of the test cell. Several tests were carried out with an experimental setup designed for testing the viability of using PCM wall integrated in building structure. The experimental study was carried out by measuring temperature through the PCM wall. The test cell indoor temperature was also evaluated to appraise the thermal inertia of the wall envelope. During the heating 22 phase, the temperature inside PCM shelter appears constant at about 28°C. But it varied between 29 and 40°C inside the test room without PCM wall.

A numerical simulation based on FORTRAN program was also carried out to interpret the experimental data. The numerical simulation was achieved to solve the energy and the exergy mathematic relations to evaluate the PCM wall performances by determining the melting phase proprieties during the charging and the discharging processes. The numerical study constitutes a preliminary step before construction of cells equipped with such wallboards in order to obtain a certain indoor passive air conditioning and especially to avoid overheating of buildings during summer. The test of the numerical model shows that there is a good agreement between experimental and numerical results. The numerical model was then exploited to evaluate the PCM wall thermal behavior. It was found that the following of the evolution of the melting front, the velocity fields, the isothermal and the current lines shows that the paraffin-27 melting process is more significant in the upper part of the PCM wall.

To generalize the investigation for a typical modern house composed of five rooms with a floor area of 128 m^2, a TRNSYS program simulation was proposed by considering the Tunisian scenario. The results were presented for a single room equipped with PCM wall. It was seen that during the day, the PCM wall stores a rate of heat that can reach 1200 kJ m^{-2}. It was found that during the hottest period of the day the temperature of the tested room with PCM wall achieves 25°C, while that without PCM wall exceeds 27°C. During the night, the temperature of the tested room, with PCM wall, is about 20°C. It is seen that the PCM wall performs its function of thermal shock absorber. The investigation showed that the efficiency of PCM wall is remarkable in the control and the reduction of the indoor temperature amplitude in the building.

The results obtained by this investigation are exploited in another new experimental work, which is in progress to optimize the geometric and the physical parameters of the PCM wall according to Tunisian buildings' specificity.

Acknowledgements

The authors would like to thank the Laboratoire des Procédés Thermiques (LPT) and the Centre de Recherches et des Technologies de l'Energie (CRTEn), Tunis, Tunisia, for financially supporting the project and for supplying useful data.

Nomenclature

A	PCM wall area (m^2)
C_{PCM}	heat capacity (kJ/kg·K)
K	thermal conductivity (W/m·K)
g	Gravitational acceleration (m/s^2)
H	Liquid fraction
L_m	enthalpy of fusion (kJ/kg)
P	pressure (Pa)

T	temperature (K)
T_i	inside air temperature (K)
T_o	outside air temperature (K)
T_{wi}	inside wall temperature (K)
T_{wo}	outside wall temperature (K)
h	Enthalpy
t	Time (s)
(x, y)	Cartesian coordinates (m)
L	cavity width
(u, v)	velocity components (m/ss^{-1})

Greek symbols

B	coefficient of thermal expansion
μ	dynamic viscosity (kg/m sm^{-1} s^{-1})
α	Thermal diffusivity coefficient
ρ	density (kg/m^3)
ν	kinematic viscosity (m^2/s)

Indices

s	Solid
l	Liquid
fus	Fusion
eq	Equivalent

Author details

Majdi Hazami[1*], Farah Mehdaoui[1], Hichem Taghouti[2], Marco Noro[3], Renato Lazzarin[3] and AmenAllah Guizani[1]

1 Laboratory of Thermal Processes, Research Center for Energy Technologies, Technopole Borj Cedria, Tunisia

2 Department of Electrical Engineering, Laboratory of Analysis, Design and Systems Control, National Engineering School of Tunis, Tunisia

3 Department of Management and Engineering, University of Padua, Vicenza, Italy

*Address all correspondence to: hazamdi321@yahoo.fr

References

[1] Mehdaoui F, Hazami M, Messaouda A, Taghouti H, Guizani A. Thermal testing and numerical simulation of PCM wall integrated inside a test cell on a small scale and subjected to the thermal stresses. Renewable Energy. 2019;**135**:597-607

[2] Solgi E, Fayaz R, Kari BM. Cooling load reduction in office buildings of hotarid climate, combining phase change materials and night purge ventilation. Renewable Energy. 2016;**85**: 725-731

[3] Lizana J, Chacartegui R, Barrios-Padura A, Valverde JM. Advances in thermal energy storage materials and their applications towards zero energy buildings: A critical review. Applied Energy. 2017;**203**:219-239

[4] Lizana J, Chacartegui R, Barrios-Padura A, Ortiz C. Advanced low-carbonenergy measures based on thermal energy storage in buildings: A review. Renewable and Sustainable Energy Reviews. 2018;**82**:3705-3749

[5] Zeinelabdein R, Omer S, Gan G. Critical review of latent heat storage systems for free cooling in buildings. Renewable and Sustainable Energy Reviews. 2018;**82**:2843-2868

[6] Reddy KS, Mudgal V, Mallick TK. Review of latent heat thermal energy storage for improved material stability and effective load management. Journal of Energy Storage. 2018;**15**:205-227

[7] Weinläder H, Klinker F, Yasin M. PCM cooling ceilings in the energy efficiency center – Passive cooling potential of two different system designs. Energy and Buildings. 2016;**119**: 93-100

[8] Soares N, Gaspar AR, Santos P, Costa JJ. Multi-dimensional optimization of the incorporation of PCM-drywalls in lightweight steel-framed residential buildings in different climates. Energy and Buildings. 2014;**70**: 411-421

[9] Navarro L, De Gracia A, Castell A, Cabeza LF. Experimental evaluation of a concrete core slab with phase change materials for cooling purposes. Energy and Buildings. 2016;**116**:411-419

[10] Zhou G, Mengmeng PM. Experimental investigations on the performance of a collector–storage wall system using phase change materials. Energy Conversion and Management. 2015;**105**:178-188

[11] Barzin R, Chen J, Young B, Farid M. Application of PCM energy storage in combination with night ventilation for space cooling. Applied Energy. 2015;**158**: 412-421

[12] Sajjadian SM, Lewis J, Sharples S. The potential of phase change materials to reduce domestic cooling energy loads for current and for future UK climates. Energy and Buildings. 2015;**93**:83-89

[13] Royon L, Karim L, Bontemp A. Optimization of PCM embedded in a floor panel developed for thermal management of the lightweight envelope of buildings. Energy and Buildings. 2014;**82**:385-390

[14] Łukasz W, Maciej J. Computer simulations of heat transfer in a building integrated heat storage unit made of PCM composite. Thermal Science and Engineering Progress. 2017;**2**:109-118

[15] Xiaoming C, Quan Z, Zhiqiang JZ, Xiaowei M. Potential of ventilation systems with thermal energ y storage using PCMs applied to air conditioned buildings. Renewable Energy. 2019; **138**:39-53

[16] Stropnik R, Koželj R, Zavrl E, Uro S. Improved thermal energy storage for nearly zero energy buildings with PCM integration. Solar Energy. 2019;**190**: 420-426

[17] Pushpendra K, Singh R, Shailendra KS. Potential of macroencapsulated pcm for thermal energy storage in buildings: A comprehensive review. Construction and Building Materials. 2019;**225**: 723-744

[18] Li D, Zheng Y, Liu C, Wu G. Numerical analysis on thermal performance of roof contained PCM of a single residential building. Energy Conversion and Management. 2015;**100**: 147-156

[19] Joulin A, Younsi Z, Zalewski L, Lassue S, Rousse DR, Cavrot JP. Experimental and numerical investigation of a phase change material: Thermal-energy storage and release. Applied Energy. 2011;**88**:2454-2462

[20] Huang K, Feng G, Zhang J. Experimental and numerical study on phase change material floor in solar water heating system with a new design. Solar Energy. 2014;**105**:126-138

[21] Prieto C, Cooper P, Fernández AI, Cabeza LF. Review of technology: Thermochemical energy storage for concentrated solar power plants. Renewable and Sustainable Energy Reviews. 2016;**60**:909-929

[22] Krese G, Butala V, Stritih U. Thermochemical seasonal solar energy storage for heating and cooling of buildings. Energy and Buildings. 2018; **164**:239-253

[23] Tasnim SH, Hossain R, Mahmud S, Dutta A. Convection effect on the melting process of nano-PCM inside porous enclosure. International Journal of Heat and Mass Transfer. 2015;**85**: 206-210

[24] Park JH, Lee J, Wi S, Jeon J, Chang SJ, Chang JD, et al. Optimization of phase change materials to improve energy performance within thermal comfort range in the South Korean climate. Energy and Buildings. 2019; **185**:12-25

[25] Fořt J, Trník A, Pavlíková M, Pavlík Z, Černy R. Fabrication of dodecanol/diatomite shape-stabilized PCM and its utilization in interior plaster. International Journal of Thermophysics. 2018;**39**(12):137

[26] Zhang C, Zhang Z, Ye R, Gao X, Ling Z. Characterization of $MgCl_2$ $6H_2O$ based eutectic/expanded perlite composite phase change material with low thermal conductivity. Materials. 2018;**11**(12):2369

[27] Ye R, Zhang C, Sun W, Fang X, Zhang Z. Novel wall panels containing $CaCl_2$ $6H_2O$-Mg $(NO_3)_2$ $6H_2O$/ expanded graphite composites with different phase change temperatures for building energy savings. Energy and Buildings. 2018;**176**:407-417

[28] Ramakrishnan S, Wang X, Sanjayan J. Thermal enhancement of paraffin/hydrophobic expanded perlite granular phase change composite using graphene nanoplatelets. Energy and Buildings. 2018;**169**:206-215

[29] Sarı A, Bicer A, Al-Ahmed A, Al-Sulaiman FA, Zahir MH, Mohamed SA. Silica fume/capric acid-palmitic acid composite phase change material doped with CNTs for thermal energy storage. Solar Energy Materials & Solar Cells. 2018;**179**:353-361

[30] Aadmi M, Karkri M, El Hammouti M. Heat transfer characteristics of thermal energy storage for PCM (phase change material) melting in horizontal tube: Numerical and experimental investigations. Energy. 2015;**85**:339-352